

See discussions, stats, and author profiles for this publication at: <https://www.researchgate.net/publication/259397521>

Atomic Details of Interfacial Interaction in Gold Nanoparticles Supported on MgO(001)

ARTICLE *in* JOURNAL OF PHYSICAL CHEMISTRY LETTERS · DECEMBER 2013

Impact Factor: 7.46 · DOI: 10.1021/jz4022975

CITATIONS

5

READS

94

3 AUTHORS:



[Yisong Han](#)

University of Cambridge

45 PUBLICATIONS 330 CITATIONS

[SEE PROFILE](#)



[Riccardo Ferrando](#)

Università degli Studi di Genova

234 PUBLICATIONS 8,376 CITATIONS

[SEE PROFILE](#)



[Ziyou Li](#)

University of Birmingham

82 PUBLICATIONS 1,343 CITATIONS

[SEE PROFILE](#)

Atomic Details of Interfacial Interaction in Gold Nanoparticles Supported on MgO(001)

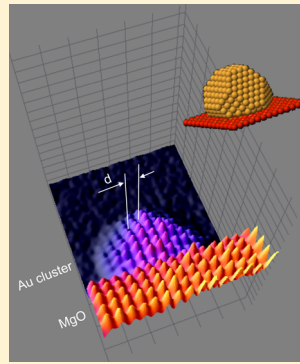
Y. Han,^{†,§} R. Ferrando,[‡] and Z. Y. Li*,[†]

[†]Nanoscale Physics Research Laboratory, School of Physics and Astronomy, University of Birmingham, Birmingham B15 2TT, United Kingdom

[‡]Dipartimento di Fisica, Università di Genova and CNR/IMEM, via Dodecaneso 33, 16146 Genova, Italy

Supporting Information

ABSTRACT: Atomic-scale imaging using aberration-corrected scanning transmission electron microscopy reveals direct evidence for semicoherent interfacial epitaxy and coordinate-dependent surface contraction for the fcc (001) oriented Au nanoparticles (2–3 nm in diameter), suggesting that their interaction with the substrate is weaker than previously assumed. A significant change in interfacial separation distance from 2.47 ± 0.12 Å for the fcc (001) oriented Au nanoparticles to 3.07 ± 0.11 Å for the fcc (111) oriented Au nanoparticles has also been observed. These results are used to verify the atomistic models generated by the global optimization calculations, which shed further light on the intricate relation between the interfacial energy and the atomic structure of the nanoparticle and their combined effect on the inhomogeneous surface structural relaxation of supported nanoparticles.



SECTION: Surfaces, Interfaces, Porous Materials, and Catalysis

Gold (Au) clusters or nanoparticles on oxide surfaces have been a subject of active scientific research, partly because of the realization of their high catalytic activity for low-temperature CO oxidation over a decade ago.^{1,2} Despite the extensive effort devoted to this subject to date, there is still much debate regarding the origin of the catalytic reactions. This is because while it has been generally accepted that the catalytic properties depend on cluster size, other factors have also been shown to play important roles. These include the availability of low-coordination Au atoms,³ the perimeter sites at the Au–oxide interface,⁴ the shape of the Au clusters,⁵ the effect of the substrate-induced strain⁶ and the intrinsic strain,⁷ and the stability of Au clusters against sintering under the reaction conditions.⁸ In addition, the catalytic properties of ultrasmall Au clusters have been attributed to the charge transfer from oxygen vacancies in MgO(001), highlighting the importance of the atomic adsorption sites.⁹ Because more than one of these mechanisms may occur simultaneously in catalytic reactions, it is crucial to understand the supported nanoclusters and the cluster/oxide interfaces at the atomic level, both experimentally and theoretically.

Among the many combinations of metals and oxides, Au on insulating MgO surfaces has been studied extensively as a model system.^{10–12} The MgO(001) surface provides a simple four-fold symmetry with alternating O and Mg atoms. They are well-characterized and can be produced with a very low defect density.¹³ The equilibrium structures of Au clusters on MgO(001) have been predicted by theoretical calculations. Accordingly, up to 10–15 atoms, they adopt two-dimensional

upright configurations.^{14,15} As the size increases, they have either an open pyramidal hollow cage or tetrahedral structures.¹⁶ Above 40 atoms, the compact fcc (001) clusters prevail, with a transition from the fcc (001) orientation to fcc (111) orientation expected to occur at around 1000 atoms (about 3 nm in diameter).¹⁷ Although the exact locations of the crossovers have not been experimentally verified, both fcc (001) and (111) oriented clusters have been imaged by transmission electron microscopy (TEM) in the size range of 1–5 nm.^{18–23} In particular, high-resolution TEM imaging has shown that the fcc (001) Au nanoparticles are coherently accommodated on the MgO(001) substrate.^{19–23} An in-plane lattice dilation of the Au lattice of ~3% was identified by electron diffraction (the lattice parameter of bulk Au is 4.08 Å, and that of MgO is 4.21 Å), although the diffraction data have been averaged over all of the Au nanoparticles.¹⁸ Overall, it has been realized that Au clusters exhibit highly size-dependent structures as a result of the complex interplay of Au–Au and Au–MgO interactions. However, very little is known experimentally about the interface where Au atoms are in direct proximity to the MgO surface. Technically, this is a challenging task as there are very limited experimental tools allowing us to have access to such information at the atomic scale, in addition to the restrictions imposed as a result of the intrinsic structural instability of nanoclusters.^{24–26}

Received: October 23, 2013

Accepted: December 10, 2013

Published: December 10, 2013



In the present work, we take a combined approach of aberration-corrected scanning transmission electron microscopy (Cs-corrected STEM) and computer simulation using global optimization with an atomistic model to study Au nanoparticles on MgO(001) in the size range where the fcc (001) and fcc (111) orientations energetically compete with each other.¹⁷ The Cs-corrected STEM enables the direct observations and analysis of the atomic column positions in both Au nanoparticles and the MgO support with an unprecedented sub-Angstrom precision.²⁷ Our aim is to shed light on the following issues. First, we seek direct evidence of the adsorption sites of Au on MgO(001) flat terraces. Second, we characterize the structure of Au nanoparticles of both (001) and (111) orientations, with special attention to the interfacial structure between Au and MgO and to the atomic relaxations in the Au particles. We find that interfacial separation is significantly different in these two orientations, and we also show a coordination-dependent inward contraction of Au atoms. The experimental results are compared to those of atomistic modeling, with a good agreement obtained.

Magnesium oxide crystals were prepared by burning magnesium ribbons in air, with the resulting MgO smoke collected on holey carbon films. MgO forms nanometer-sized cubes exposing only the low-energy {100} surfaces, as shown in Figure 1a. Au nanoparticles were formed on the MgO surfaces at 300 °C through thermal evaporation in a vacuum chamber (2×10^{-7} mbar). Before the evaporation, the MgO crystals were degassed under the high-vacuum condition for more than 1 h in

order to release the absorbed hydrocarbon species on the surfaces. The nanoparticles were imaged using a JEOL 2100F STEM equipped with a CEOS probe aberration corrector and operated at 200 kV. The semiconvergence angle for the electron beam was ~20 mrad. High-angle annular dark-field (HAADF) STEM images were taken using a JEOL annular dark-field detector with an inner and outer collection angle of 55 and 148 mrad, respectively. An overview of one of the samples is shown in the Supporting Information (Figure S1), where the top and side surfaces of the MgO cubes were covered by Au nanoparticles. The Au particles prepared in this experiment have an average diameter of about 2–3 nm, with a dominant fcc (001) orientation with respect to the MgO (001) substrate. This orientation relationship is described as $(001)_{\text{Au}}//(001)_{\text{MgO}}$ and $[100]_{\text{Au}}//[100]_{\text{MgO}}$. A small percentage of the nanoparticles adopt the fcc (111) orientation, being described as $(111)_{\text{Au}}//(001)_{\text{MgO}}$ and $[110]//[110]_{\text{MgO}}$. The prevalence of the (001) orientation in this size range agrees with the results of atomistic modeling, as previously reported.¹⁷

Figure 1b shows schematics of Au nanoparticles on MgO (001) viewed along either the [001] or [011] direction of MgO within the microscope. Plan-view (type 1,3) or cross-sectional (type 2,4) images may be recorded depending on where the nanoparticles are located. Figure 1c is a HAADF-STEM image of a fcc (001) orientated Au particle, and Figure 1d is the same image processed by fast Fourier transform (FFT) and then inverse FFT to improve visualization. In this alignment of the MgO crystal, the bright spots in the MgO image correspond to pure Mg columns, while the dark region between two neighboring Mg columns corresponds to pure O columns. Although oxygen atoms are not visible directly in the HAADF image because of its relatively smaller atomic number and the Z-contrast nature of the HAADF-STEM imaging mode,^{28,29} it is apparent that the Au atoms at the interface are preferentially located above the sites between two Mg columns. When viewing a particle along the [100] direction (Figure 2a), Au (200) atomic columns are seen in approximate register with the (200) columns of the MgO substrate. The combined information from both viewing directions provides direct experimental evidence confirming the previous theoretical predictions that gold atoms on regular MgO(001) surfaces prefer to bind on oxygen sites,^{30–33} and it also agrees with the experimental results from scanning tunneling microscopy and electron paramagnetic resonance spectroscopy.³⁴

The atomically resolved image of the fcc (001) oriented Au nanoparticle taken along the [001] direction of MgO in Figure 2a enables us to perform a detailed strain analysis, which is an extremely challenging task for particles of this size. While the geometric phase analysis (GPA), developed from high-resolution TEM, is well-established to study the lattice strain in thin films or nanoparticles of tens of nanometers, the validity of this method for small nanoparticles of a few nanometers is still debatable.³⁵ In this study, the local lattice spacings were measured directly from the as-taken HAADF-STEM images. The atomic spacing inside of the bulk of the MgO substrate was used as a standard for an absolute scale. Briefly, a 5 pixel line was drawn parallel to the spacing in question to extract the corresponding intensity profile, as in the inset of Figure 2a. The peaks in the intensity profile were then fitted by Gaussian functions, from which a lattice spacing was measured as being the distance between the maxima of two neighboring Gaussian functions. It is noted that there have been reports about the MgO lattice expansions of 0.1% when the crystal dimension is

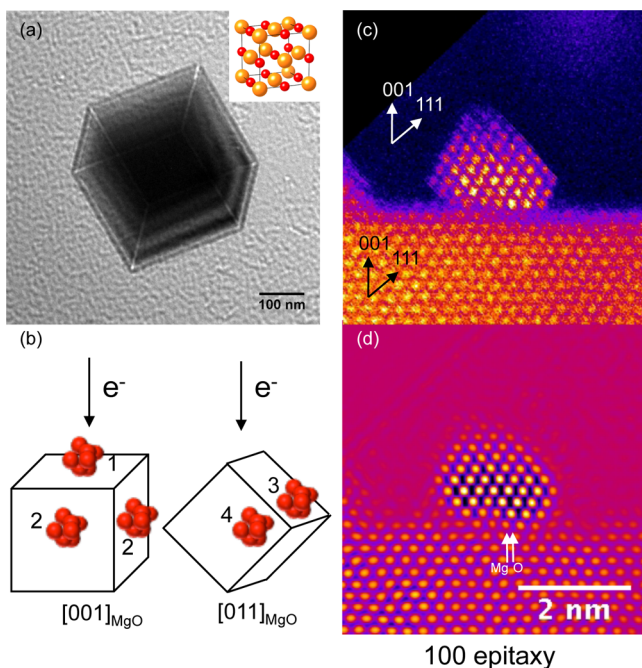


Figure 1. (a) TEM image of a MgO cube, with a MgO lattice model shown in the inset. (b) Schematics of Au nanoparticles on MgO(001) viewed along the [001] and [011] directions of MgO within the microscope. Plan-view (type 1,3) and cross-sectional (type 2,4) images can be acquired depending on where the nanoparticles are located on MgO. (c) HAADF-STEM image from a (001) oriented nanoparticle, taken along the [110] direction of MgO. (d) Filtered image using FFT followed by inverse FFT. On MgO, the bright spots correspond to the Mg columns, with the dark regions between two neighboring spots to the O columns. It is clear that for the fcc (001) nanoparticle, the Au atoms are strictly located on top of the oxygen atoms.

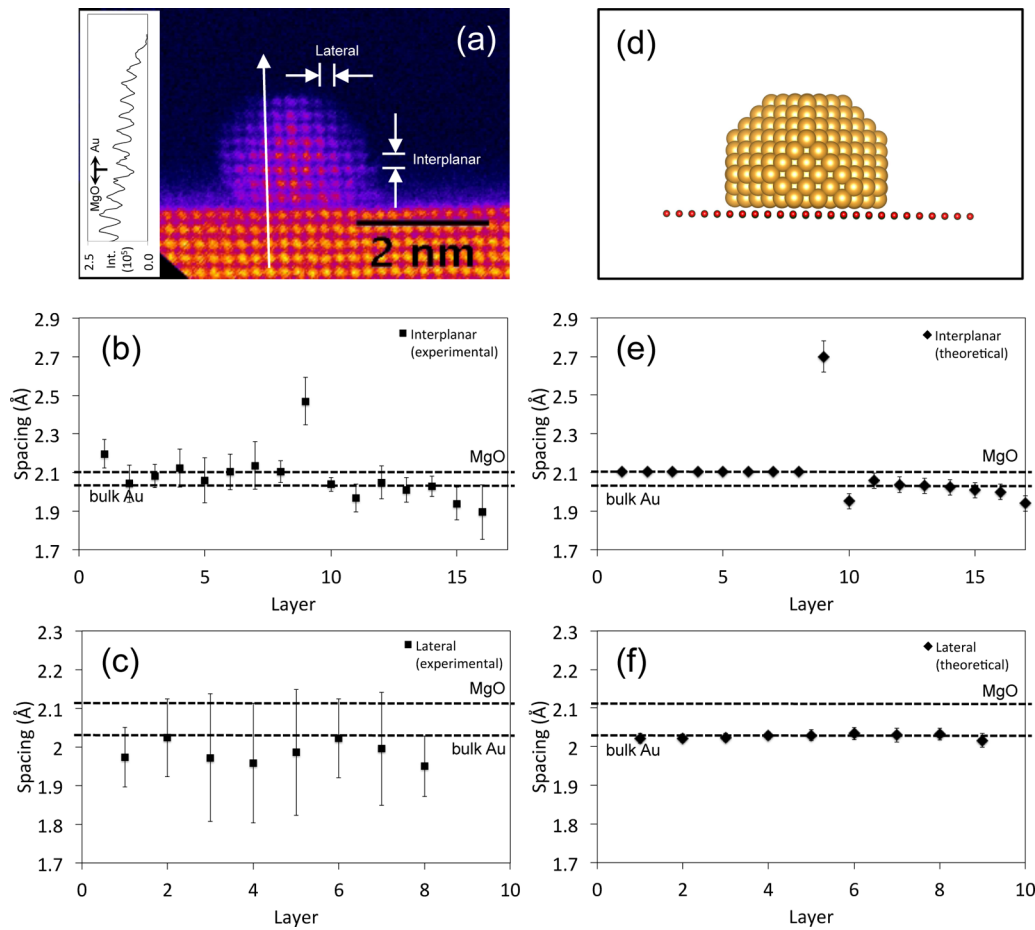


Figure 2. (a) HAADF-STEM images taken along the [001] zone axis of MgO from a fcc (001) nanoparticle. The inset is the intensity profile acquired from the marked line in (a). (b,c) Average interplanar and lateral spacings measured from (a), plotted with reference to the layer positions. (d) 2D projection of the structural model containing 500 Au atoms calculated using the global optimization techniques for the fcc (100) oriented nanoparticles on MgO (001), viewed along the (100) direction of MgO. (e,f) Variations of average interplanar and lateral spacings measured directly from the structural model in (d).

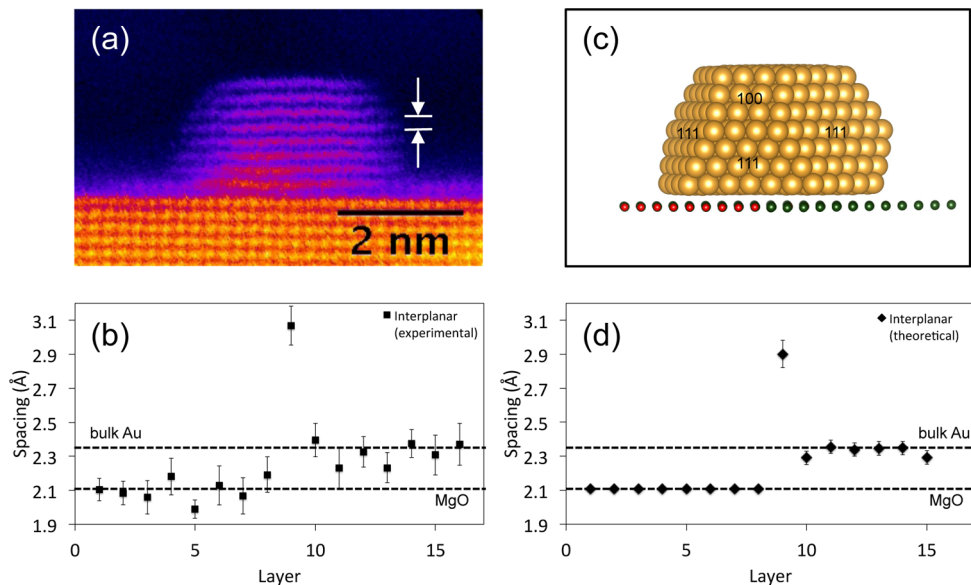


Figure 3. (a) HAADF-STEM images taken along the [001] zone axis of MgO from a fcc (111) nanoparticle. (b) Variation of the interplanar lattice spacing measured directly from (a). (c) 2D projection of the calculated structural model along the [001] direction of MgO. (d) Variation of the interplanar lattice spacing measured from the structural model in (c).

less than 50 nm.³⁶ However, the typical size of the MgO cubes observed in this work is around 100–200 nm (Figures 1a and S1, Supporting Information); hence, it is expected that the lattice parameter of the MgO cubes measured is close to the bulk value.

We discovered that the in-plane strain of the gold nanoparticle is inhomogeneously distributed. To aid the discussion, we first analyzed the experimental results in terms of two types of lattice spacings, interplanar spacing (between the lattice planes parallel to the interface) and lateral spacings (lattice spacing within a plane parallel to the interface). Figure 2b,c shows, respectively, the average (002) interplanar and lateral spacings from this fcc (001) nanoparticle, plotted with reference to the atomic layer concerned away from the Au/MgO interface. The error bars shown are the standard deviations calculated from the same sets of data. The data points (in Figure 2b) with $n \leq 8$ belong to the MgO substrate, and the (002) lattice spacings of bulk Au and MgO are marked by the dashed lines. The interface distance between the first layer of Au and the MgO surface is measured as 2.47 ± 0.12 Å. The most prominent feature here is an inward contraction of the Au nanoparticle, with its magnitude varied depending on how far away the atom is from the interface. The contraction at the topmost layer of the particle reaches 1.90 ± 0.14 Å, corresponding to a contraction of 6.9% of the bulk value. However, the lateral spacings plotted in Figure 2c suggest that the Au particle takes on the bulk Au lattice parameter immediately at the Au/MgO interface.

Figures 3a shows a HAADF-STEM image of a fcc (111) oriented Au nanoparticle on the MgO(001) surface. The interplanar spacings from the experiment are again plotted with reference to the MgO interface in Figures 3b. Compared to the interfacial spacing of 2.47 Å from the fcc (001) oriented nanoparticle, a much larger value of 3.07 ± 0.11 Å is observed. Also, no apparent trend of atomic contraction was detected experimentally in Figure 3b in the fcc (111) nanoparticle, with the interplanar spacings varying slightly around the corresponding bulk value.

To gain further insight into the observed phenomena, we conducted theoretical calculations of the structures of Au₅₀₀ (a cluster consisting of 500 Au atoms) on MgO(001) surfaces for both fcc (001) and (111) clusters using a global optimization method within an atomistic potential model.¹⁷ The choice of the clusters, with the same size for both orientations, is to single out the effects of cluster orientation in the interfacial separation distance. Here, Au–Au interactions are modeled by a second-moment tight-binding potential, whereas the Au–MgO interactions are fitted to DFT calculations.³⁷ The global optimization searches have been performed by the basin-hopping algorithm and its variants.³⁸ For each cluster, at least 5 runs of 2×10^5 Monte Carlo steps have been performed.

The calculated structural model along the [100] direction of the MgO is shown in Figure 2d. In order to compare directly with the experimental results, both interplanar and lateral lattice spacings extracted from the model are converted into the corresponding 2D projections, averaged and shown in Figure 2e,f. As in the experimental data, we see a large Au/MgO interfacial spacing from the (001) orientated model structure at 2.70 ± 0.08 Å and a larger gap of 2.90 ± 0.08 Å for the (111) orientated cluster (Figure 3c,d). The result is comparable with the Au–O bond length of 2.8 Å, as reported from DFT calculations of the extended deposition of one or two monolayers of Au on MgO(001).³⁹ The interfacial lattice

spacing results from both the experiments and calculations are summarized in Table 1. It should be pointed out that the same

Table 1. Comparison of Interplanar Distance between Au and the MgO(100) Plane

interface type	Au–MgO(001)
Experimental Data	
Au _{2.0} nm: (100) _{Au} /(100) _{MgO}	2.47 ± 0.12
Au _{2.5} nm: (111) _{Au} /(100) _{MgO}	3.07 ± 0.11
Theoretical Data	
Au ₅₀₀ : (100) _{Au} /(100) _{MgO}	2.70 ± 0.08
Au ₅₀₀ : (111) _{Au} /(100) _{MgO}	2.90 ± 0.08
Au _{2 ML} : (100) _{Au} /(100) _{MgO}	2.8 ^a

^aDFT calculation results. The data are taken from ref 39.

number of atoms, $N = 500$, was used in the calculation in both cases. In practice, the fcc (111) clusters appear in a larger size regime than the fcc (001) clusters. This may contribute partially to the larger interfacial distance observed from the fcc (111) cluster in the experiments than that in the calculations. Possible point defects on the MgO(001) surfaces,⁴⁰ which cannot be observed in profiling STEM imaging, may contribute to stronger initial binding of Au on surface, hence the reduced bonding length observed from the (001) cluster in experiments.³⁹ The simulations have also reproduced the surface contraction of the Au atoms at the topmost layers as well as at the interface for the fcc (001) oriented cluster. It is further shown by the modeling that the degree of the surface contraction is smaller for the (111) oriented Au cluster than that for the (001) cluster, being 0.06 Å. Such a small value may have approached our current experimental limit due to the signal-to-noise and signal-to-background ratios of the STEM images and/or due to the larger Debye–Waller factors exhibited by the surface atoms.⁴¹ Overall, the above results show, for the first time, that the interaction between the Au cluster and MgO(001) is dependent on the atomic structure of the cluster in direct proximity to the MgO surface.

In situ grazing-incidence small-angle X-ray scattering using synchrotron radiation has been demonstrated to be a powerful technique in the study of real-time nanoparticle behaviors during growth and chemical reactions, which can provide averaged information across a sample, such as particle size and shape.^{42–44} Previously, the atomic details, such as lateral lattice spacings, in Au nanoparticles supported on MgO(001) were measured from electron diffraction patterns¹⁸ and high-resolution TEM images.²² Unlike the data shown here, it was found that Au nanoparticles were well-accommodated on the MgO surfaces, adopting a dilated spacing close to that of MgO. However, the lattice spacing reported by electron diffraction is an averaged value from single nanoparticles, which smears out the contribution from surface atoms.¹⁸ In addition, non-aberration-corrected TEM imaging is known to be unreliable for locating the atomic sites at the surface of nanoparticles²² and for measuring the separation distance between MgO and Au nanoparticles. The latter situation is because the image contrast in high-resolution TEM images is highly sensitive to the sample thickness and objective lens defocus. In the present study, the spherical aberration-corrected HAADF images provide us an unprecedented opportunity for identifying directly the atomic sites with high accuracy. The key message obtained from our unambiguous measurements is that the

epitaxial $(100)_{\text{Au}}/\!/ (001)_{\text{MgO}}$ interface is semicoherent, contrary to previous claims.^{18–23} Our results indicate that the interaction between Au nanoparticles and the MgO substrate is rather weak and the surface relaxation seen at the free (001) surface also survives partially at the interface.

Although the profiling Cs-STEM imaging is a powerful tool in gaining atomistic information at the interface, its 2D projection nature does not allow us to study coordination-dependent atomic relaxation of supported Au nanoparticles. However, the structural models, calculated by molecular dynamics simulation and validated by the available observation data, enable us to learn more about the three-dimensional arrangements of the atoms. Figure 4a,b shows the 3D structural

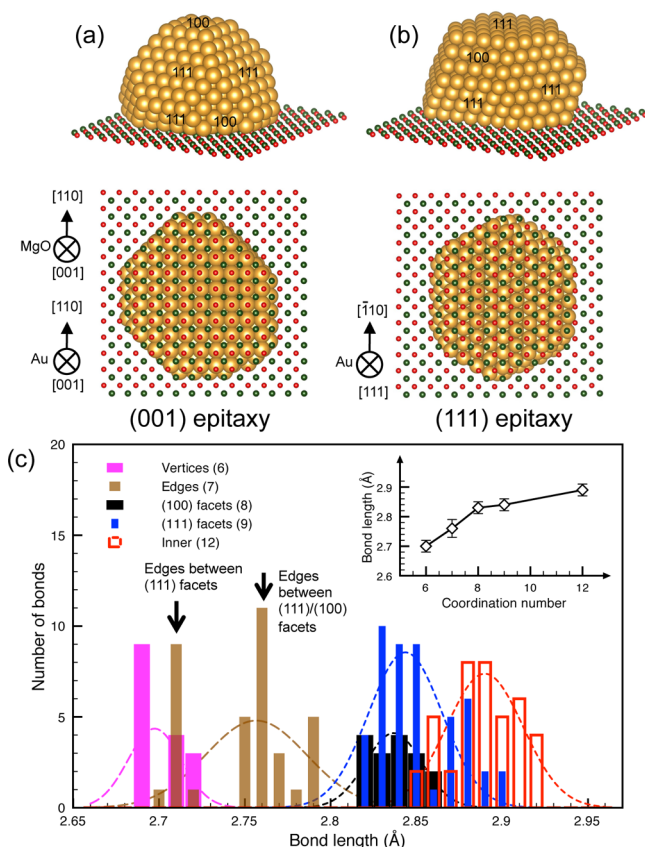


Figure 4. (a,b) 3D view of the calculated models having the (001) or (111) orientation, respectively. The exposed facets are labeled in each case. The models are also shown in a bottom view from the MgO side. (c) Distribution of the out-of-plane Au–Au bond lengths for the surface atoms measured from the calculated model. Bond lengths for atoms further inside of the nanoparticle, with both end atoms having a coordination number of 12, are also presented for comparison. The data points are grouped according to the coordination number of the surface Au atoms (given in brackets) and fitted with Gaussian functions. The inset displays the mean value of the bond length as a function of coordination number.

models where the exposed (100) and (111) facets are labeled. The same models viewed from the MgO side are also shown in both cases. The Au–Au out-of-plane bond lengths involving the surface atoms are obtained from the fcc (001) Au_{500} structural model. They are grouped according to the coordination numbers of the corresponding surface atoms and presented using a histogram in Figure 4c. In a fcc lattice, a Au atom with a complete shell is surrounded by 12 other Au

atoms, while a vertex atom has a coordination number of 6. The bonds inside of the model between Au atoms, both with a coordination number of 12, are also included in this figure for comparison. Each set of data in Figure 4c is fitted by a Gaussian function, with the resultant mean bond length as a function of coordination number plotted in the inset. An increase in bond length with increasing coordination number is revealed. Accordingly, the shortest bond length is associated with the vertex atoms being 2.70 ± 0.02 Å, and the longest bond length is associated with the inner bonds being 2.89 ± 0.02 Å, which is already the value for bulk Au of 2.88 Å. The peaks for the bonds associated with the (100) and (111) facets are very much located at the same values. It is worth mentioning that the data with a coordination number of 7 in fact consist of two peaks (brown), one belonging to the atoms at the edges defined by the neighboring (111) facets and the other to those by the neighboring (100) and (111) facets. This indicates that the bonds at the saddles between (111) facets are shortened significantly, and they are at the same level as those of the vertex atoms.

The fundamental observations in this work, including the difference in interfacial spacing and the difference in surface contraction between the fcc (001) orientated nanoparticles and the fcc (111) orientated nanoparticles on MgO(001), are the direct results of the weak interaction between the Au nanoparticle and the MgO surface as well as the reduced out-of-plane Au–Au bonds associated with the surface atoms. Figure 4a shows that the top (001) layer of the cluster is made up of $4 \times 4 = 16$ atoms. Among them, four are vertex atoms and eight are edge atoms, with the remaining four being pure (100) facet atoms. The presence of a large percentage of the vertex and edge atoms leads to the smallest average bond length and thus the smallest topmost (002) lattice spacing. The effect of the contracted bonds is increasingly diluted for the rest of the interplanar (002) spacings toward the Au/MgO interface, resulting in the gradual increase in lattice spacing. This can also explain the smaller lattice contraction in the top layer of the fcc (111) nanoparticle (Figure 3), which is evidenced by the model. In this case, the effect of surface bond contraction is further weakened in view of the percentage of the vertex and edge atoms, for example, 19 in 42 as counted from the fcc (111) structural model.

In summary, we provide evidence in this study on the semicoherent nature of the interfaces separating the fcc Au nanoparticles and the surface of the MgO(001) substrate. We have shown experimentally for the first time, confirmed by calculation, that the interfacial separation distance is sensitive to the orientation of the nanoparticles supported on the MgO(001) surface. Together with the observed surface contraction of the Au nanoparticles, it is suggested that the Au–MgO interaction, although sufficiently large enough to stabilize the fcc structured Au nanoparticles on the preferential oxygen sites on MgO, is still too weak to overcome the inward surface contraction of the nanoparticles as has been observed on fcc Au nanoparticles supported on an amorphous carbon thin film.^{45,46} The findings of this study may have potential implications relating to oxide-supported Au nanocatalysts. Finally, we have demonstrated that a combined approach of experiment and simulation is an indispensable tool in the study of the 3D structure of supported nanoparticles as the latter can provide insight that sometimes cannot be gained by experiments alone.

■ ASSOCIATED CONTENT

§ Supporting Information

STEM images showing an overview of Au nanoparticles formed on MgO cubes. This material is available free of charge via the Internet at <http://pubs.acs.org>.

■ AUTHOR INFORMATION

Corresponding Author

*E-mail: z.li@bham.ac.uk.

Present Address

[§]Y.H.: Department of Materials Science and Metallurgy, University of Cambridge, 27 Charles Babbage Road, Cambridge CB3 0FS, U.K.

Notes

The authors declare no competing financial interest.

■ ACKNOWLEDGMENTS

The authors acknowledge the Engineering and Physical Sciences Research Council U.K. (EPSRC) for financial support (Grant No.: EP/G070326/1) and the COST Action MP0903. The Cs-corrected STEM used in this project was partially funded by the Birmingham Science City project (AWM).

■ REFERENCES

- (1) Haruta, M. Gold as a Novel Catalyst in the 21st Century: Preparation, Working Mechanism and Applications. *Gold Bull.* **2004**, *37*, 27–36.
- (2) Haruta, M.; Yamada, N.; Kobayashi, T.; Iijima, S. Gold Catalysts Prepared by Coprecipitation for Low-Temperature Oxidation of Hydrogen and of Carbon-Monoxide. *J. Catal.* **1989**, *115*, 301–309.
- (3) Lopez, N.; Janssens, T. V. W.; Clausen, B. S.; Xu, Y.; Mavrikakis, M.; Bligaard, T.; Norskov, J. K. On the Origin of the Catalytic Activity of Gold Nanoparticles for Low-Temperature CO Oxidation. *J. Catal.* **2004**, *223*, 232–235.
- (4) Cargnello, M.; Doan-Nguyen, V. V. T.; Gordon, T. R.; Diaz, R. E.; Stach, E. A.; Gorte, R. J.; Fornasiero, P.; Murray, C. B. Control of Metal Nanocrystal Size Reveals Metal–Support Interface Role for Ceria Catalysts. *Science* **2013**, *341*, 771–773.
- (5) Molina, L. M.; Hammer, B. Active Role of Oxide Support During CO Oxidation at Au/MgO. *Phys. Rev. Lett.* **2003**, *90*, 206102.
- (6) Xu, Y.; Mavrikakis, M. Adsorption and Dissociation of O₂ on Gold Surfaces: Effect of Steps and Strain. *J. Phys. Chem. B* **2003**, *107*, 9298–9307.
- (7) Walsh, M. J.; Yoshida, K.; Kuwabara, A.; Pay, M. L.; Gai, P. L.; Boyes, E. D. On the Structural Origin of the Catalytic Properties of Inherently Strained Ultrasmall Decahedral Gold Nanoparticles. *Nano Lett.* **2012**, *12*, 2027–2031.
- (8) Yan, W. F.; Mahurin, S. M.; Pan, Z. W.; Overbury, S. H.; Dai, S. Ultrastable Au Nanocatalyst Supported on Surface-Modified TiO₂ Nanocrystals. *J. Am. Chem. Soc.* **2005**, *127*, 10480–10481.
- (9) Yoon, B.; Hakkinen, H.; Landman, U.; Worz, A. S.; Antonietti, J. M.; Abbet, S.; Judai, K.; Heiz, U. Charging Effects on Bonding and Catalyzed Oxidation of CO on Au₈ Clusters on MgO. *Science* **2005**, *307*, 403–407.
- (10) Freund, H. J. Clusters and Islands on Oxides: From Catalysis via Electronics and Magnetism to Optics. *Surf. Sci.* **2002**, *500*, 271–299.
- (11) Henry, C. R. Morphology of Supported Nanoparticles. *Prog. Surf. Sci.* **2005**, *80*, 92–116.
- (12) Marks, L. D. Experimental Studies of Small-Particle Structures. *Rep. Prog. Phys.* **1994**, *57*, 603–649.
- (13) Henry, C. R. Surface Studies of Supported Model Catalysts. *Surf. Sci. Rep.* **1998**, *31*, 231–325.
- (14) Ferrando, R.; Barcaro, G.; Fortunelli, A. Structures of Small Au Clusters on MgO(001) Studied by Density-Functional Calculations. *Phys. Rev. B* **2011**, *83*, 045418.
- (15) Molina, L. M.; Alonso, J. A. Chemical Properties of Small Au Clusters: An Analysis of the Local Site Reactivity. *J. Phys. Chem. C* **2007**, *111*, 6668–6677.
- (16) Ferrando, R.; Barcaro, G.; Fortunelli, A. Surface-Supported Gold Cages. *Phys. Rev. Lett.* **2009**, *102*, 216102.
- (17) Ferrando, R.; Rossi, G.; Levi, A. C.; Kuntova, Z.; Nita, F.; Jelea, A.; Mottet, C.; Barcaro, G.; Fortunelli, A.; Goniakowski, J. Structures of Metal Nanoparticles Adsorbed on MgO(001). I. Ag and Au. *J. Chem. Phys.* **2009**, *130*, 174702.
- (18) Giorgio, S.; Chapon, C.; Henry, C. R.; Nihoul, G.; Penisson, J. M. High-Resolution Transmission Electron-Microscopy Study of Gold Particles (Greater Than 1 nm), Epitaxially Grown on Clean MgO Microcubes. *Philos. Mag. A* **1991**, *64*, 87–96.
- (19) Giorgio, S.; Henry, C. R.; Chapon, C.; Nihoul, G.; Penisson, J. M. Electron-Beam-Induced Transformations of Gold Particles Epitaxially Grown on MgO Microcubes. *Ultramicroscopy* **1991**, *38*, 1–12.
- (20) Kizuka, T.; Tanaka, N. Atomic Process of Epitaxial Growth of Gold on Magnesium Oxide Studied by Cross-Sectional Time-Resolved High-Resolution Electron Microscopy. *Phys. Rev. B* **1997**, *56*, 10079–10082.
- (21) Kizuka, T.; Kachi, T.; Tanaka, N. Effect of Interface on Structural Fluctuation in Gold Clusters Fixed on MgO Fine Rods. *Z. Phys. D* **1993**, *26*, S58–S60.
- (22) Pauwels, B.; Van Tendeloo, G.; Bouwen, W.; Kuhn, L. T.; Lievens, P.; Lei, H.; Hou, M. Low-Energy-Deposited Au Clusters Investigated by High-Resolution Electron Microscopy and Molecular Dynamics Simulations. *Phys. Rev. B* **2000**, *62*, 10383–10393.
- (23) Giorgio, S.; Cabie, M.; Henry, C. R. Dynamic Observations of Au Catalysts by Environmental Electron Microscopy. *Gold Bull.* **2008**, *41*, 167–173.
- (24) Han, Y.; He, D. S.; Liu, Y.; Xie, S.; Tsukuda, T.; Li, Z. Y. Size and Shape of Nanoclusters: Single-Shot Imaging Approach. *Small* **2012**, *8*, 2361–2364.
- (25) Li, Z. Y.; Young, N. P.; Di Vece, M.; Palomba, S.; Palmer, R. E.; Bleloch, A. L.; Curley, B. C.; Johnston, R. L.; Jiang, J.; Yuan, J. Three-Dimensional Atomic-Scale Structure of Size-Selected Gold Nanoclusters. *Nature* **2008**, *451*, 46–48.
- (26) Han, Y.; He, D. S.; Li, Z. Y. Direct Observation of Dynamic Events of Au Clusters on MgO(100) by HAADF-STEM. *J. Nanopart. Res.* **2013**, *15*, 1941.
- (27) Van Tendeloo, G.; Bals, S.; Van Aert, S.; Verbeeck, J.; Van Dyck, D. Advanced Electron Microscopy for Advanced Materials. *Adv. Mater.* **2012**, *24*, 5655–5675.
- (28) Akita, T.; Kohyama, M.; Haruta, M. Electron Microscopy Study of Gold Nanoparticles Deposited on Transition Metal Oxides. *Acc. Chem. Res.* **2013**, *46*, 1773–1782.
- (29) Li, Z. Y. Scanning Transmission Electron Microscopy Studies of Mono- and Bimetallic Nanoparticles. In *Frontiers of Nanosciences: Metal and Nanoalloys*, Johnston, R. L., Wilcoxon, J. P., Eds.; Elsevier: New York, 2012; Vol. 3.
- (30) Ferrando, R.; Fortunelli, A. Diffusion of Adatoms and Small Clusters on Magnesium Oxide Surfaces. *J. Phys.: Condens. Matter* **2009**, *21*, 264001.
- (31) Neyman, K. M.; Inntam, C.; Nasluzov, V. A.; Kosarev, R.; Rosch, N. Adsorption of D-Metal Atoms on the Regular MgO(001) Surface: Density Functional Study of Cluster Models Embedded in an Elastic Polarizable Environment. *Appl. Phys. A* **2004**, *78*, 823–828.
- (32) Chen, D.; Ma, X. L.; Wang, Y. M. First-Principles Study of the Interfacial Structures of Au/MgO(001). *Phys. Rev. B* **2007**, *75*, 125409.
- (33) Cheng, D.; Lan, J.; Wang, W.; Cao, D. Theoretical Study of the Structures of MgO(100)-Supported Au Clusters. *Surf. Sci.* **2009**, *603*, 881–886.
- (34) Yulikov, M.; Sterrer, M.; Heyde, M.; Rust, H. P.; Risse, T.; Freund, H. J.; Pacchioni, G.; Scagnelli, A. Binding of Single Gold Atoms on Thin MgO(001) Films. *Phys. Rev. Lett.* **2006**, *96*, 146804.
- (35) Johnson, C. L.; Snoeck, E.; Ezcurdia, M.; Rodríguez-González, B.; Pastoriza-Santos, I.; Liz-Marzáñ, L. M.; Hýtch, M. J. Effects of

Elastic Anisotropy on Strain Distributions in Decahedral Gold Nanoparticles. *Nat. Mater.* **2007**, *7*, 120–124.

(36) Cimino, A.; Porta, P.; Valigi, M. Dependence of the Lattice Parameter of Magnesium Oxide on Crystallite Size. *J. Am. Ceram. Soc.* **1966**, *49*, 152–156.

(37) Vervisch, W.; Mottet, C.; Goniakowski, J. Theoretical Study of the Atomic Structure of Pd Nanoclusters Deposited on a MgO(100) Surface. *Phys. Rev. B* **2002**, *65*, 245411.

(38) Rossi, G.; Ferrando, R. Searching for Low-Energy Structures of Nanoparticles: A Comparison of Different Methods and Algorithms. *J. Phys.: Condens. Matter* **2009**, *21*, 084208.

(39) Barcaro, G.; Fortunelli, A. The Interaction of Coinage Metal Clusters with the MgO(100) Surface. *J. Chem. Theory Comput.* **2005**, *1*, 972–985.

(40) Barth, C.; Henry, C. R. Atomic Resolution Imaging of the (001) Surface of UHV Cleaved MgO by Dynamic Scanning Force Microscopy. *Phys. Rev. Lett.* **2003**, *91*, 196102.

(41) Peng, L. M.; Ren, G.; Dudarev, S. L.; Whelan, M. J. Debye-Waller Factors and Absorptive Scattering Factors of Elemental Crystals. *Acta Crystallogr., Sect. A* **1996**, *52*, 456–470.

(42) Nolte, P.; Stierle, A.; Jin-Phillipp, N. Y.; Kasper, N.; Schulli, T. U.; Dosch, H. Shape Changes of Supported Rh Nanoparticles during Oxidation and Reduction Cycles. *Science* **2008**, *321*, 1654–1658.

(43) Renaud, G.; Lazzari, R.; Revenant, C.; Barbier, A.; Noblet, M.; Ulrich, O.; Leroy, F.; Jupille, J.; Borensztein, Y.; Henry, C. R.; Deville, J. P.; Scheurer, F.; Mane-Mane, J.; Fruchart, O. Real-Time Monitoring of Growing Nanoparticles. *Science* **2003**, *300*, 1416–1419.

(44) Schwartzkopf, M.; Buffet, A.; Koerstgens, V.; Metwalli, E.; Schlage, K.; Benecke, G.; Perlich, J.; Rawolle, M.; Rothkirch, A.; Heidmann, B.; Herzog, G.; Mueller-Buschbaum, P.; Roehlsberger, R.; Gehrke, R.; Stribeck, N.; Roth, S. V. From Atoms to Layers: In Situ Gold Cluster Growth Kinetics During Sputter Deposition. *Nanoscale* **2013**, *5*, 5053–5062.

(45) Mitome, M.; Takayanagi, K.; Tanishiro, Y. Commensurate Reconstruction on a (001) Facet of a Gold Particle. *Phys. Rev. B* **1990**, *42*, 7238–7241.

(46) Huang, W. J.; Sun, R.; Tao, J.; Menard, L. D.; Nuzzo, R. G.; Zuo, J. M. Coordination-Dependent Surface Atomic Contraction in Nanocrystals Revealed by Coherent Diffraction. *Nat. Mater.* **2008**, *7*, 308–313.